Exploiting PV Inverters to Support Local Voltage—A Small-Signal Model

Meghdad Fazeli, *Member, IEEE*, Janaka B. Ekanayake, *Senior Member, IEEE*, Paul M. Holland, *Member, IEEE*, and Petar Igic, *Member, IEEE*

***Abstract*—As penetration of distributed generation increases, the electrical distribution networks may encounter several challenges mainly related to voltage control. The situation may deteriorate in case of a weak grid connected to an intermittent source such as photovoltaic (PV) generation. Fast varying solar irradiance can cause unacceptable voltage variations that may not be easily compensated by slow-responding utility equipment. The PV inverter can be used to control the grid voltage by injecting/absorbing reactive power. A small-signal model is derived in order to study the stability of a PV inverter exchanging reactive power with the grid. This paper also proposes a method that utilizes the available capacity of the PV inverter to support the grid voltage without violating the rating of the inverter and the maximum voltage that the inverter's switching device can withstand. The method proposed in this paper is validated using PSCAD/EMTDC simulations.**

***Index Terms*—Distributed generation (DG), photovoltaic (PV) system, voltage control.**

I. Introduction

DISTRIBUTED generation (DG) benefits the electric utility by reducing congestion on the grid, decreasing the need for new generation and transmission capacity and (potentially) can offer services such as local frequency and voltage support/control [1]–[5]. However, as penetration of renewable-based DG increases, the intermittent nature of the source can cause challenges such as voltage variations which in turn can lead to system instability [6]. Yan and Saha [7] investigate the IEEE 13 nodes test system with different level of photovoltaic (PV) penetrations and show for a penetration more than 40%; the voltage fluctuations introduced by passing clouds may make the system unstable. In such situations, the slow-responding equipment (e.g., tap changers or switchable capacitors) may not be effective in controlling the voltage within its limits [6], [8]. For instance, it takes 5–10 s for the tap changer to move from one position to the next [7]. Relying on the tap changer in a fast varying irradiance condition, (assuming is practically possible) will also significantly reduce the interval between maintenance and increases the cost [9]. In addition to the slow response and the fact that capacitor banks can generate high frequency harmonics, switching the capacitor banks on/off produces a strong transient voltage variation that can damage other equipment (e.g., PV inverters) [6]. On the other hand, installing fast-responding FACTS devices (e.g., STATCOM, SVC, etc.) will increase the cost of already expensive PV systems [6]. Alternatively, it is possible to utilize the PV inverter in order to control the voltage within its limits through absorbing/injecting reactive power.

"Although it is not permitted by current interconnection standard [8], changes to these standards to allow for injecting or consuming reactive power appear eminent" [6].

The allowed penetration level of (PV) DG is a controversial issue among scientists [10] and varies from 5% [11], [12] to 33% [13] in the literature. Quezada *et al.* [12] suggest that the loss in a distribution system is minimized at 5% penetration of DG. However, the findings of [12] can be doubted if the reactive power capacity of the PV inverter is exploited. For instance, Turitsyn *et al.* [14] show that a localized approach to supply reactive power (e.g., using PV inverters) can reduce losses by up to 80% when compared to a centralized approach. Thomson and Infield [13] study the voltage rise issue versus the penetration level of PV generation into a UK distribution network and conclude that for a PV generation up to 33%, the voltage rise is within acceptable limits. However, Thomson and Infield [13] also show that even at 50% penetration of PV generation, the voltage rise above the allowed limit is small and hence the 33% is rather arbitrary. From the findings of [13], it can be suggested that by exploiting the PV inverters to support the local voltage, it is possible to increase the penetration of PV generation by more than 33%. It is noted that Thomson and Infield [13] study the voltage rise issue due to a high penetration of PV generation and it states that the voltage dips caused by passing clouds can be significant. The current paper studies a distribution system with 50% penetration of PV generation (since it seems the maximum level suggested by the literature [13]).

Turitsyn *et al.* [6] propose a voltage-reactive power droop that utilizes the PV inverter to support voltage. The main drawback of the proposed method in [6] is that the reactive power exchanged by the inverter never becomes zero even when the voltage is within an acceptable boundary (which may introduce unnecessary losses). A similar method is proposed in [7] with zero reactive power boundary; however, the mathematical model of the system has not been investigated. Moreover, these methods do not take into account the voltage rise issue due to

Manuscript received July 5, 2013; revised November 18, 2013; accepted December 16, 2013. This work was sponsored by European Regional Development Fund through Welsh European Funding Office, Welsh Government. Paper no. TEC-00380-2013.

M. Fazeli, P. M. Holland, and P. Igic are with the Electronic Design Center, College of Engineering, Swansea University, Swansea SA2 9HD, U.K. (e-mail: m.fazeli@swansea.ac.uk; p.m.holland@swansea.ac.uk; p.igic@swansea.ac.uk).

J. B. Ekanayake is with the School of Engineering, Cardiff University, Cardiff CF24 3AA, U.K. (e-mail: ekanayakej@cardiff.ac.uk).

Color versions of one or more of the figures in this paper are available online at http://ieeexplore.ieee.org.

Digital Object Identifier 10.1109/TEC.2014.2300012

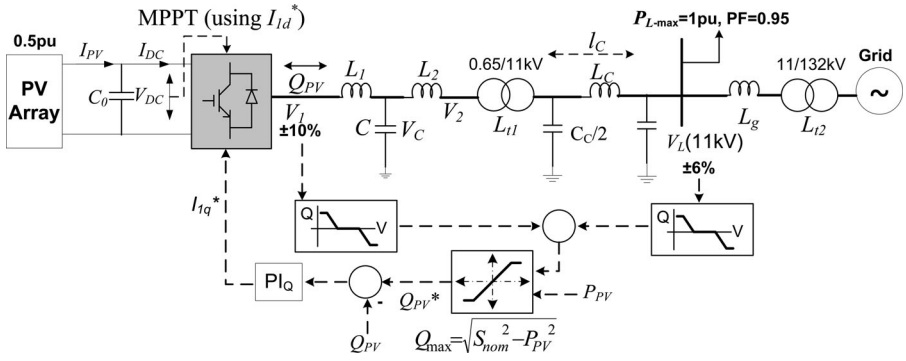

Fig. 1. Configuration of the system under study.

the reverse active and reactive power flow. Beside the possibility of exceeding the voltage limits, the voltage rise introduced by PV inverters may cause "overmodulation" [15] (i.e., modulation index > 1), and even may harm the switching device (for a constant dc-link voltage).

The papers in this area, such as [6], [7], [16], [17], do not study the small-signal stability of a PV inverter exchanging reactive power with the grid; which will be considered in this paper. The paper also proposes a method that utilizes the available capacity of the PV inverter(s) to support the grid voltage without violating the rating of the inverter and the maximum voltage that the inverter's switching device can withstand.

The method will be developed for one PV inverter and will be demonstrated for multiple PV inverters as well, using PSCAD/EMTDC simulations.

II. System Under Study

Fig. 1 shows the configuration of the system under study. It illustrates that the PV array can supply maximum 50% of the full load (at solar irradiation $G = 1$ kW/m^2). The PV system utilizes a single stage conversion using a three-phase dc/ac converter. The converter is controlled using a *dq* rotating frame with the d axes orientated along the filter voltage V_2. The d-component current controls the dc-link voltage $V_{\rm DC}$ in order to track the maximum solar power (using the method explained in [18]) and the q-component controls the reactive power to/from the converter. Park transformation is used to transfer variables from *abc* to *dq* frame [19]. l_C is the length of the cable connecting the PV system to the grid and L_1, L_2, and C represent the filter and L_g is the grid inductance.

A. Problem Definition

It can be shown that without any voltage support, the voltage of point of common coupling $V_L < 0.94$ pu for short-circuit ratio (SCR) < 15 and in fact it drops to 0.87 pu for SCR $= 5$. On the other hand, keeping V_L at 1 pu using the PV inverter will cause the inverter ac terminal voltage V_1 to increase even more than 1.2 pu. Therefore, a variable approach to control V_L, as illustrated in Fig. 1, seems to be more appropriate. The proposed method exploits the available capacity of the PV inverter to support the local voltage without violating either the rating of the inverter or its voltage limitations. As $Q_{\rm PV}$ varies, both V_1 and the load voltage V_L will be affected. Therefore, it is important to choose a proper reactive power reference $Q^*_{\rm PV}$. In order to choose a proper $Q^*_{\rm PV}$, the following constraints are considered.

1) Voltage of 11 kV busbar V_L should be within ±6% (i.e., 0.94 pu $\leq V_L \leq$ 1.06 pu) [20].
2) The maximum voltage that the switching device can withstand is 10% of its rated value (i.e., $V_1 \leq 1.1$ pu).
3) Rating of the inverter $S_{\rm nom}$ should not be violated. Here $S_{\rm nom} = 1.2$ pu$_{\rm pv}$ (pu$_{\rm pv}$ denotes pu based on the rating of the associated PV array in systems with multiple PV arrays).

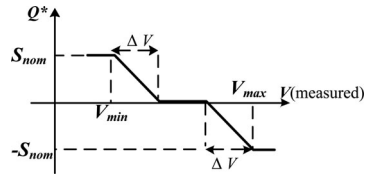

Fig. 2. Proposed Q–V droop characteristic.

B. Control Paradigm

Fig. 1 illustrates the proposed method to set $Q^*_{\rm PV}$ in order to support V_L (if required) without violating $S_{\rm nom}$ and V_1. The method consists of three parts.

1) A PI controller which controls $Q_{\rm PV}$ through regulating the q-component of converter current I_{1q}, and is explained in Section VI.
2) A variable hard limit which limits $Q^*_{\rm PV}$ to makes sure $S_{\rm nom}$ is not exceeded.
3) Since the PV power $P_{\rm PV}$ is intermittent, the maximum reactive power that can be exchanged by the inverter is varying as: $Q_{\max} = \sqrt{S^2_{\rm nom} - P^2_{\rm PV}}$, hence a variable hard limit is required. Using the variable hard limit also makes sure that the voltage support does not interfere with the maximum power tracking.

Two reactive power-voltage droop characteristics for V_L and V_1 as shown in Fig. 1 and illustrated in Fig. 2. These droops provide the opportunity to keep $Q_{\rm PV} = 0$ when the voltage is within an acceptable boundary.

Fig. 2 illustrates the droop characteristics used for both V_L and V_1; however, $V_{\min}$ and $V_{\max}$ are different for each voltage.

$V_{\max}$ for V_1 and V_L is 1.1 and 1.06 pu, respectively. $V_{\min}$ for $V_{\rm PV}$ and V_L is 0.9 and 0.94 pu, respectively. As ΔV reduces, the droop's gain increases (for a given $S_{\rm nom}$) which requires a $Q_{\rm PV}$ control loop with higher bandwidth (which can cause large voltage transient). On the other hand, the smaller ΔV, the larger the boundary with zero reactive power (which reduces the losses). So the choice of ΔV is a tradeoff between less loss and less transient. Here, ΔV is chosen as 0.02 pu for both droops; however, it can be different for V_1 and V_L droops.

It is noted that since the power flows from PV to the load, V_1 is on the right side of Fig. 2 (negative Q) while V_L is on the left side (positive Q). The output of the two droop characteristics is added together and fed to the variable hard limit (hence, supporting V_L cannot lead to V_1 overvoltage and vice versa). Using this method, the maximum capacity of the converter is demanded for reactive power support when $V \le V_{\min}$ or $V \ge V_{\max}$; however, the support will be fully provided only if the other voltage (i.e., V_L or V_1) is $(V_{\min} + \Delta V) \le V \le (V_{\max} - \Delta V)$, and the variable hard limit (i.e., $S_{\rm nom}$) is not exceeded.

III. Mathematical Model of the System

This part is intended to drive a small-signal model for a PV system exchanging reactive power with the grid. The model is derived for any operating point of $P_{\rm PV0}$ and $Q_{\rm PV0}$. The model will be used to study the stability of the system later on in the paper.

A. PV Array

This part is intended to linearize a PV array model around an operating point $P_{\rm PV0}$, which is assumed to be its maximum power point (at a given solar irradiation).

The mathematical model of PV array current $I_{\rm PV}$ is given by (1) and explained in [21]:

$$I_{\rm PV} = N_p I_{\rm ph} - N_p I_{\rm rs}\left[\exp\left(\frac{qV_{\rm DC}}{k{\rm TAN}_s}\right) - 1\right] \quad (1)$$

where N_p and N_s are the number of parallel and series connected cells, $I_{\rm rs}$ is the reverse saturation current of a p–n junction (1.2 $\times$ 10^{-7}A), q is the unit electric charge (1.602 $\times$ 10^{-19}C), k is Boltzman's constant (1.38 $\times$ 10–23 J/K), T is the p–n junction temperature (Kelvin), A is the ideally factor (1.92) and $I_{\rm ph}$, which is the short-circuit current of one string of the PV panel, is a function of T and G [21]:

$$I_{\rm ph} = \frac{G}{100}\left[I_{\rm scr} + k_T\left(T - T_r\right)\right] \quad (2)$$

where T_r is the cell reference temperature (300 K), K_T is temperature coefficient (0.0017 A/K), $I_{\rm scr}$ is the short-circuit current of one PV cell at the reference temperature (8.03 A) and G is the solar irradiation level normalized to 1 kW/m^2 [21]. Equation (1) is nonlinear and needs to be linearized. For a given G and T, $I_{\rm ph}$ is a constant. Hence, (1) can be linearized as follows:

$$\hat{I}_{\rm PV} = \frac{-N_p I_{\rm rs} q}{k{\rm TAN}_s}\left[\exp\left(\frac{qV_{\rm DC0}}{k{\rm TAN}_s}\right)\right]\hat{V}_{\rm DC} = K_{\rm PV}\hat{V}_{\rm DC}. \quad (3)$$

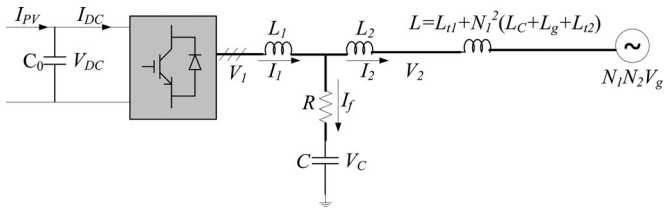

Fig. 3. Simplified model of a grid-connected PV system.

Hereafter the variables with subscript "0" and superscript "^" denote the operating point and the small-signal variables, respectively.

According to (3), $K_{\rm PV}$ is a function of $V_{\rm DC0}$. So it is required to calculate $V_{\rm DC0}$ in terms of the operating point of PV system.

From the method explained in [18], it can be shown that for a given PV array, $V_{\rm DC}$ at maximum power points can be approximated as an order 3 polynomial of $P_{\rm PV}$:

$$V_{\rm DC0} = aP_{\rm PV0}^3 + bP_{\rm PV0}^2 + cP_{\rm PV0} + d. \quad (4)$$

Knowing the $i_{\rm pv} - v_{\rm pv}$ characteristic of a PV array (which can be obtained from the manufacturer), it is possible to calculate the coefficients a, b, c, and d using Matlab "polyfit" command [18].

B. Average Model of the Inverter

Fig. 3 illustrates a simplified version of Fig. 1 in order to derive the mathematical model. The load active and reactive powers can be neglected as they appear as disturbances for the inverter controller. The cable is represented by its inductance L_C and all of the inductances are transferred to the PV filter side (i.e., $L = L_{t1} + (L_C + L_g + L_{t2})N_1^2$, $N_1 = 0.65/11$, $N_2 = 11/132$).

Using sinusoidal pulse-width modulation (PWM) and considering only the fundamental frequency, the average model of the inverter in *dq* frame is:

$$I_{\rm DC} = m_d I_{1d} + m_q I_{1q} \quad (5)$$

$$V_{1d} = 0.5 m_d V_{\rm DC}$$

$$V_{1q} = 0.5 m_q V_{\rm DC} \quad (6)$$

where m is the magnitude of the modulation index.

Equations (5) and (6) are linearized as follow:

$$\hat{I}_{\rm DC} = m_{d0}\hat{I}_{1d} + m_{q0}\hat{I}_{1q} + \hat{m}_d I_{1d0} + \hat{m}_q I_{1q0} \quad (7)$$

$$\hat{V}_{1d} = 0.5\left(m_{d0}\hat{V}_{\rm DC} + \hat{m}_d V_{\rm DC0}\right)$$

$$\hat{V}_{1q} = 0.5\left(m_{q0}\hat{V}_{\rm DC} + \hat{m}_q V_{\rm DC0}\right). \quad (8)$$

C. Filter and the Grid

The series resistance of the filter inductors is neglected and a damping resistor R is connected in series with the filter capacitor.

Using KVL one can write:

$$V_1 = L_1\frac{dI_1}{dt} + RI_f + V_C. \quad (9)$$

Transferring (9) into *dq* frame and taking into account $I_f = I_1 - I_2$ and then substituting (8) into the result, gives:

$$\frac{d\hat{I}_{1d}}{dt} = \omega\hat{I}_{1q} + \frac{0.5\left(m_{d0}\hat{V}_{\rm DC} + \hat{m}_d V_{\rm DC0}\right)}{L_1} - \frac{R}{L_1}\left(\hat{I}_{1d} - \hat{I}_{2d}\right) - \frac{V_{\rm Cd}}{L_1} \tag{10}$$

$$\frac{d\hat{I}_{1q}}{dt} = -\omega\hat{I}_{1d} + \frac{0.5\left(m_{q0}\hat{V}_{\rm DC} + \hat{m}_q V_{\rm DC0}\right)}{L_1} - \frac{R}{L_1}\left(\hat{I}_{1q} - \hat{I}_{2q}\right) - \frac{V_{\rm Cq}}{L_1}. \tag{11}$$

It can be written from the dc-link circuit:

$$C_0\frac{dV_{\rm DC}}{dt} = I_{\rm PV} - I_{\rm DC}. \tag{12}$$

Transferring (12) into *dq* frame and substituting (3) and (7) into it, yield:

$$\frac{d\hat{V}_{\rm DC}}{dt} = -\frac{m_{d0}\hat{I}_{1d} + m_{q0}\hat{I}_{1q} + \hat{m}_d I_{1d0} + \hat{m}_q I_{1q0}}{C_0} + \frac{K_{\rm PV}\hat{V}_{\rm DC}}{C_0}. \tag{13}$$

Transferring the filter capacitor's current equation into *dq* frame and taking into account that $I_f = I_1 - I_2$, give:

$$\frac{d\hat{V}_{\rm Cd}}{dt} = \omega\hat{V}_{\rm Cq} + \frac{\hat{I}_{1d} - \hat{I}_{2d}}{C} \tag{14}$$

$$\frac{d\hat{V}_{\rm Cq}}{dt} = -\omega\hat{V}_{\rm Cd} + \frac{\hat{I}_{1q} - \hat{I}_{2q}}{C}. \tag{15}$$

Using KVL one can write:

$$-V_C - R\left(I_1 - I_2\right) + L_2\frac{dI_2}{dt} + V_2 = 0. \tag{16}$$

Transferring (16) into *dq* yield:

$$\frac{d\hat{I}_{2d}}{dt} = \omega\hat{I}_{2q} + \frac{\hat{V}_{\rm Cd}}{L_2} + \frac{R}{L_2}\left(\hat{I}_{1d} - \hat{I}_{2d}\right) - \frac{\hat{V}_{2d}}{L_2} \tag{17}$$

$$\frac{d\hat{I}_{2q}}{dt} = -\omega\hat{I}_{2d} + \frac{\hat{V}_{\rm Cq}}{L_2} + \frac{R}{L_2}\left(\hat{I}_{1q} - \hat{I}_{2q}\right) - \frac{\hat{V}_{2q}}{L_2}. \tag{18}$$

One can write the space state model of the system using (10), (11), (13), (14), (15), (17), and (18):

$$\begin{aligned}
&\frac{d}{dt}\mathbf{x} = \mathbf{A}\cdot\mathbf{x} + \mathbf{B}\cdot\mathbf{u}\\
&\mathbf{Y} = \mathbf{C}\cdot\mathbf{x} + \mathbf{D}\cdot\mathbf{u}\\
&\mathbf{x} = \begin{bmatrix}\hat{I}_{1d} & \hat{I}_{1q} & \hat{V}_{\rm DC} & \hat{V}_{\rm Cd} & \hat{V}_{\rm Cq} & \hat{I}_{2d} & \hat{I}_{2q}\end{bmatrix}^{\rm T}\\
&\mathbf{u} = \begin{bmatrix}\hat{m}_d & \hat{m}_q & \hat{V}_{2d} & \hat{V}_{2q}\end{bmatrix}^{\rm T}.
\end{aligned} \tag{19}$$

Matrices **C** and **D** are used to determine output **Y** and matrices **A** and **B** are as follows:

$$\mathbf{A} = \begin{bmatrix}
\frac{R}{L_1} & \omega & \frac{0.5m_{d0}}{L_1} & \frac{-1}{L_1} & 0 & \frac{R}{L_1} & 0\\
-\omega & \frac{-R}{L_1} & \frac{0.5m_{q0}}{L_1} & 0 & \frac{-1}{L_1} & 0 & \frac{R}{L_1}\\
\frac{-m_{d0}}{C_0} & \frac{-m_{q0}}{C_0} & \frac{K_{\rm PV}}{C_0} & 0 & 0 & 0 & 0\\
\frac{1}{C} & 0 & 0 & 0 & \omega & \frac{-1}{C} & 0\\
0 & \frac{1}{C} & 0 & -\omega & 0 & 0 & \frac{-1}{C}\\
\frac{R}{L_2} & 0 & 0 & \frac{1}{L_2} & 0 & \frac{-R}{L_2} & \omega\\
0 & \frac{R}{L_2} & 0 & 0 & \frac{1}{L_2} & -\omega & \frac{-R}{L_2}
\end{bmatrix}$$

$$\mathbf{B} = \begin{bmatrix}
\frac{0.5V_{\rm DC0}}{L_1} & 0 & 0 & 0\\
0 & \frac{0.5V_{\rm DC0}}{L_{10}} & 0 & 0\\
\frac{-I_{1d0}}{C_0} & \frac{I_{1q0}}{C_0} & 0 & 0\\
0 & 0 & 0 & 0\\
0 & 0 & 0 & 0\\
0 & 0 & \frac{-1}{L_2} & 0\\
0 & 0 & 0 & \frac{-1}{L_2}
\end{bmatrix}.$$

The operating points can be calculated using (10), (11), (13), (14), (15), (17), (18), and $V_1 = L_1\frac{dI_1}{dt} + L_2\frac{dI_2}{dt} + V_2$, taking into account that at steady state $d/dt = 0$. $V_2 q = 0$, and to calculate $V_2 d$, one can write:

$$V_2 = L\frac{dI_2}{dt} + N_1 N_2 V_g. \tag{20}$$

Transferring (20) into *dq* frame, solving it for $V_{\rm gd0}$ and $V_{\rm gq0}$, and taking into account that $V_2 q = 0$, $I_{2d0} = 2P_{\rm PV0}/3V_{2d0}$, and $I_{2q0} = -2Q_{\rm PV0}/3V_{2d0}$ give:

$$V_{\rm gd0} = \frac{V_{2d0}}{N_1 N_2} - \frac{2L\omega Q_{\rm PV0}}{3N_1 N_2 V_{2d0}} \tag{21}$$

$$V_{\rm gq0} = \frac{2L\omega P_{\rm PV0}}{3N_1 N_2 V_{2d0}}. \tag{22}$$

Substituting (21) and (22) into $V_g^2 = V_{\rm gd0}^2 + V_{\rm gq0}^2$, yields, as shown (23), at the bottom of the next page.

Equation (23) gives two answers for V_{2d0}; however, the one given through subtraction is too small and is not acceptable. The equations of operating points are summarized in Table I.

IV. System's Parameters

The most effective system parameters on the open-loop poles are the filter elements and the dc-link capacitor C_0. The filter elements are chosen to reduce the current ripples down to a

TABLE I
CALCULATION OF OPERATING POINTS

Variable	Operating point
V_g	132kV RMS line-line
V_{2d0}	Eq (23)
V_{2q0}	0
I_{2d0}	$\frac{2P_{PV0}}{3V_{2d0}}$
I_{2q0}	$\frac{-2Q_{PV0}}{3V_{2d0}}$
I_{1q0}	$\frac{C\omega\left(RCL_2\omega^2 I_{2d0}+V_{2d0}\right)-I_{2q0}\left(L_2C\omega^2-(RC\omega)^2-1\right)}{1+(RC\omega)^2}$
I_{1d0}	$I_{2d0}\left(1-CL_2\omega^2\right)+RC\omega\left(I_{1q0}-I_{2q0}\right)$
m_{d0}	$\frac{2\left(V_{2d0}-\omega L_1 I_{1q0}-\omega L_2 I_{2q0}\right)}{V_{DC0}}$
m_{q0}	$\frac{2\left(V_{2q0}+\omega L_1 I_{1d0}+\omega L_2 I_{2d0}\right)}{V_{DC0}}$

specific requirement (THD $< 5\%$) [22]. The filter capacitance and resistance are usually chosen to be less than 5% and 1% of the rated power, respectively [22].

The choice of C_0 is very important since a small capacitor requires a very fast control loop (which increases the control energy) while a large one is bulky and expensive. So it is important to have a mathematical minimum value for C_0, which to the authors' knowledge is not provided previously and is considered in the following: Ideally $I_{\rm DC} = I_{\rm PV}$, however, due to the switching effects sometimes (whenever all the top switches are open or closed simultaneously) $I_{\rm DC} = 0$. Hence, $I_{\rm PV}$ flows through C_0: $I_{\rm PV} = C_0 \frac{\Delta V_{\rm DC}}{\Delta t}$. In a sinusoidal PWM, this happens twice in one period of carrier signal $f_{\rm sw}$, i.e., $\Delta t = 1/(2f_{\rm sw})$. Obviously the largest voltage variation happens when the nominal PV power is generated $I_{\rm PV} = P_{\rm PVnom}/V_{DCnom}$. The largest voltage variation must be less than permitted voltage variation $\Delta V_{\rm DC\,max} \geq \frac{P_{\rm PVnom}}{2f_{\rm sw}V_{\rm DCnom}C_0}$, hence $C_0 \geq \frac{P_{\rm PVnom}}{2f_{\rm sw}V_{\rm DCnom}\Delta V_{\rm DC\,max}}$, and $\Delta V_{DC\,\rm max} \leq 5\%$.

The system parameters are summarized in Table II.

TABLE II
SYSTEM'S PARAMETERS

Variable	*Value*
P_{PVnom}	1MW
V_{DCnom}	1.8kV
L_1	0.25 mH
L_2	0.11mH
L	0.3 mH
R	0.8 Ω
C	376.7 μF
C_0	1700 μF

V. VARIATION OF OPEN-LOOP POLES

The open-loop poles of the system, which are the eigenvalues of matrix **A,** vary for different system parameters and different operating points. The system parameters are set according to the criteria explained in Section IV. So this part investigates the variation of the open-loop poles for different operating points.

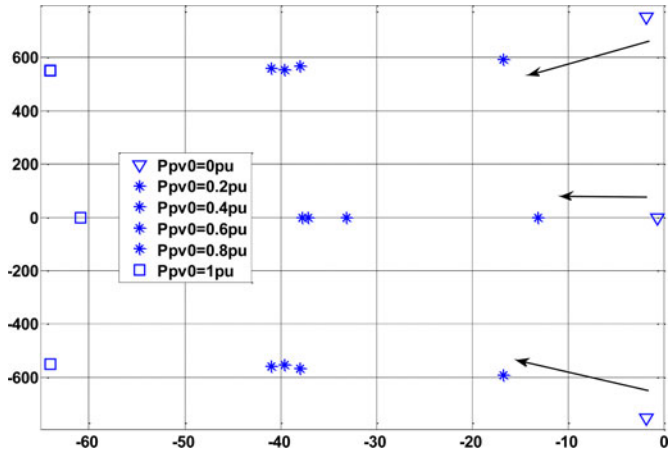

Fig. 4. Variation of open-loop poles as $P_{\rm PV0}$ varies for $Q_{\rm PV0} = 0$.

A. Different Active Power Generation

The system has one real pole and three pairs of complex conjugate poles. Two pairs of the complex conjugate poles are relatively far away from the $j\omega$ axes and change rather vertically as $P_{\rm PV}$ varies (so not shown here). Fig. 4 illustrates the variation of the other three poles as $P_{\rm PV}$ increases from 0 to 1 pu in five steps and $Q_{\rm PV} = 0$.

As shown in Fig. 4, as $P_{\rm PV}$ increases the poles move toward stability (away from $j\omega$ axes).

B. Different Reactive Power

Similar to the previous case, two pairs of the complex conjugate poles are far away from the $j\omega$ axes and vary rather vertically as $Q_{\rm PV}$ changes. Fig. 5 shows the variation of the rest of the poles as $Q_{\rm PV}$ varies from -1 to 1 pu in eight steps. As it can be seen, the complex conjugate poles move toward stability. Although the real pole moves toward $j\omega$ axes, it never crosses it (i.e., the system is stable). It is noted that the case shown in Fig. 5 is the worst since $P_{\rm PV} = 0$ (according to Fig. 4

$$V_{2d0} = \sqrt{0.5\left[1.33L\omega Q_{\rm PV0} + (N_1N_2V_g)^2 \pm \sqrt{\left[-1.33L\omega Q_{\rm PV0} - (N_1N_2V_g)^2\right]^2 - 1.78\,(L\omega)^2\,(P_{\rm PV0}{}^2 + Q_{\rm PV0}{}^2)}\right]}. \quad (23)$$

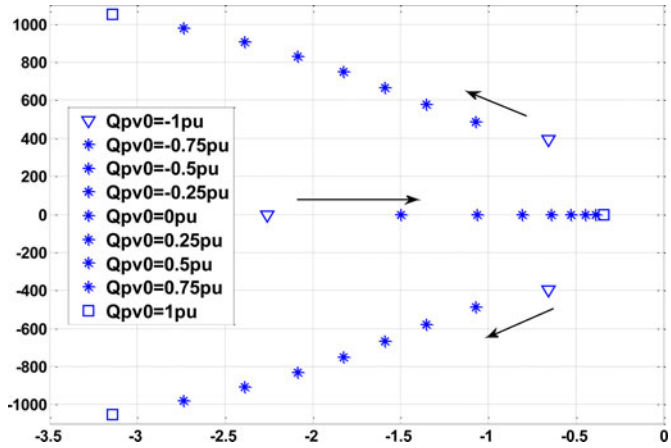

Fig. 5. Variation of open-loop poles as Q_{PV0} varies when $P_{\mathrm{PV0}} = 0$.

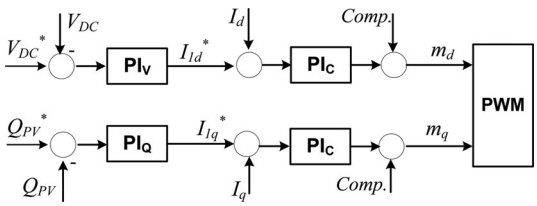

Fig. 6. Schematic diagram of inverter's control loops.

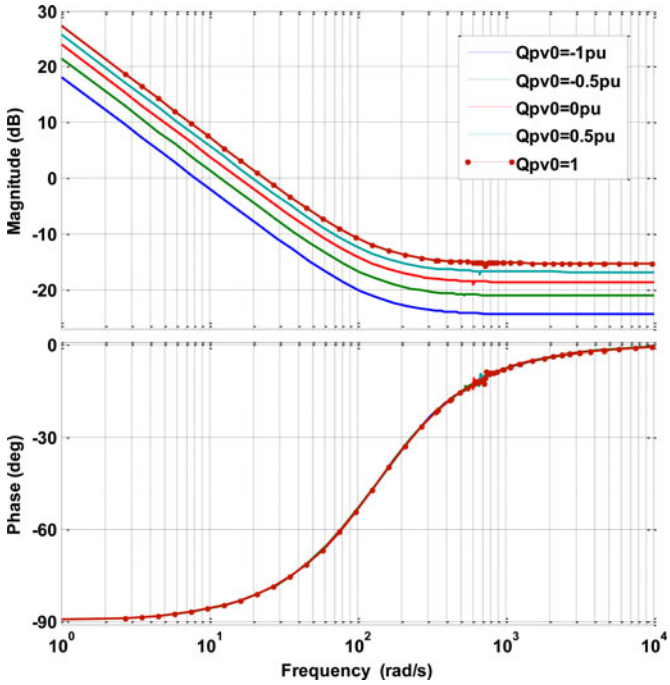

Fig. 7. Bode diagram of G_Q (s) as Q_{PV0} varies for $P_{\mathrm{PV0}} = 0$.

increasing P_{PV} moves the poles away from $j\omega$ axes). So it can be concluded that the worst case from stability point of view is when $P_{\mathrm{PV}} = 0$ and $Q_{\mathrm{PV}} = 1$ pu.

VI. Control Loop

This paper utilizes the classical cascaded control loops with the internal current loops as shown in Fig. 6.

The study and design of the current loops (PI$_C$) and the dc-link voltage control (PI$_V$) has been considered in the previous literature [19]. This paper investigates the reactive power control loop (PI$_Q$).

Neglecting the filter, since $V_{2q} = 0$, $Q_{\mathrm{PV}} \approx -1.5 I_1 q V_{2d}$. So assuming $V_2 d$ is constant, the control plant of the reactive power control loop is a constant gain of $-0.67/V_{2d}$.

In such cases, trial and error can be used to design the control loop which is done in this paper using Matlab "sisotool" facility. The proportional and integral gains of PI$_Q$ are set 0.0015 and 0.02, respectively. The stability of Q_{PV} control loop can be studied by the reactive power control loop gain $G_Q(s)$ explained as follows:

$$G_Q(s) = \mathrm{PI}_Q(s) \frac{I_{1q}(s)}{I_{1q}^*(s)} \frac{Q_{\mathrm{PV}}(s)}{I_{1q}(s)}. \tag{24}$$

Since the internal current loop is much faster than the external reactive power loop, $\frac{I_{1q}(s)}{I_{1q}^*(s)} \approx 1$. The exact transfer function of $\frac{Q_{\mathrm{PV}}(s)}{I_{1q}(s)}$ is calculated using Matlab "ss2tf" command. Fig. 7 illustrates the Bode diagram of G_Q(s) as Q_{PV} varies from -1 to 1 pu in four steps. Since it was shown in Section V that the worst case for stability happens when $P_{\mathrm{PV}} = 0$, in Fig. 7 the active power generation is kept at zero. Fig. 7 shows that the system always has a good stability margin (phase margin $> 95^\circ$ and infinite gain margin).Therefore, it can be concluded that the reactive power control loop does not affect the system stability.

VII. Simulation Results

Fig. 8 shows the simulated model using PSCAD. The model consists of two PV arrays of 0.3 and 0.2 pu ratings while the rating of their associated converter is $S_{\mathrm{nom}} = 1.2$ pu$_{\mathrm{pv}}$ (unless otherwise stated). The PV system feeds the 1 pu load (i.e., 50% PV penetration) connected to the 11 kV busbar. The grid SCR is 5 (i.e., a weak grid it can be shown that V_L drops down to 0.87 pu without voltage support). The first PV system (0.3 pu) connected to the load with 10-km cable while the other one is connected to the load with 5-km cable. Each PV system has its own *V–Q* control (explained above). Therefore, the two PV systems share the control of V_L while their converter ratings and each V_{PV} must not be violated. Three different scenarios are simulated: the first two scenarios apply four-step changes to solar irradiation while the third considers real (measured) solar irradiation profiles. It is assumed in the first scenario that both PV arrays have the same solar irradiation while in the second and third scenarios different solar irradiations are applied.

A. Same Solar Irradiation for Both PV Arrays

Table III illustrates the sequence of simulation events. At first $P_L = 1$ pu with Power Factor PF = 0.95 and P_{PV} increases from 0 to 1 pu$_{\mathrm{pv}}$ in four steps. At $t = 5$ s, the load PF drops to 0.85 and backs to 0.95 at $t = 6.5$ s. At $t = 8$ s P_L reduces from 1 pu to 0 in four steps. Fig. 9 shows the simulation results of the two PV systems with the same solar irradiation. It can be seen that when

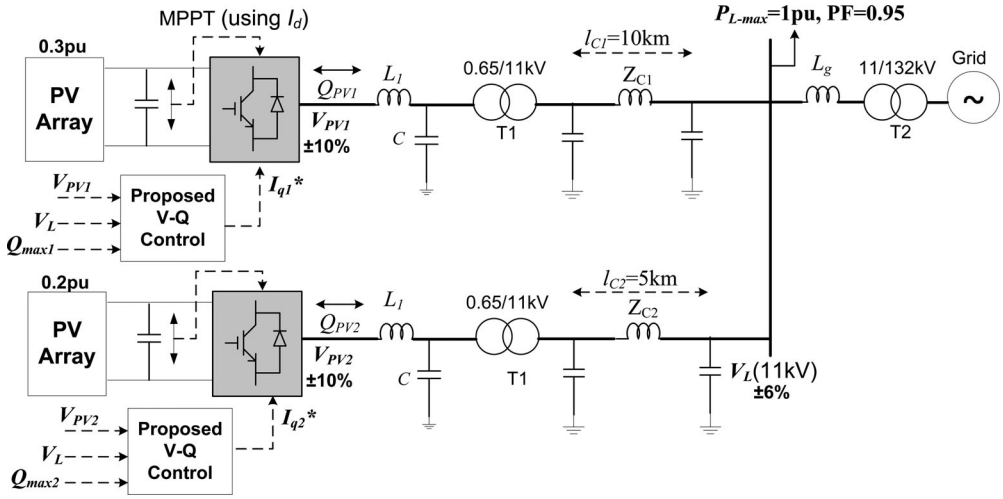

Fig. 8. Simulated model with two PV arrays sharing the control/support of V_L using the proposed *V–Q* droop.

TABLE III
SEQUENCE OF SIMULATION EVENTS FOR THE SAME IRRADIATION SCENARIO

Time, s	P_L, pu	P_{PV}, pu_{pv}	Load PF
0-1	1	**0**	0.95
1-2	1	**0.25**	0.95
2-3	1	**0.5**	0.95
3-4	1	**0.75**	0.95
4-5	1	**1**	0.95
5-6.5	1	1	**0.85**
6.5-8	1	1	**0.95**
8-9	**0.75**	1	0.95
9-10	**0.5**	1	0.95
10-11	**0.25**	1	0.95
11-12	**0**	1	0.95

PF drops to 0.85 (i.e., t = 5–6.5 s), V_L [see Fig. 9(b)] drops to less than 0.92 pu (which is less than the minimum limits) while the magnitudes of the inverters' apparent power [see Fig. 9(d)] increase to 1.2 pu_{pv}. This means that the two inverters provide the maximum possible support without violating their ratings. Fig. 9(b) shows that for both inverters $V_{PV} < 1.1$ pu. V_{PV1} is more than V_{PV2} simply because more active and reactive powers flow from P_{V1} to the load.

Fig. 9(c) illustrates that the reactive power demanded by load Q_L is shared proportionally by the inverter (i.e., Q_{PV1}/Q_{PV2} = 3/2). Fig. 9(c) shows that for $P_L < 0.5$ pu, Q_{PV1} and Q_{PV2} are almost zero since all the three voltages are $(V_{min} + \Delta V) \le V \le (V_{max} - \Delta V)$. Fig. 10 illustrates the simulation results with the same sequence of simulation events (see Table III) but this time the converter ratings are $S_{nom} = 1.5$ pu_{pv}. It can be seen that even when PF = 0.85 (t = 5–6.5 s), $V_L > 0.94$ pu while both V_{PV1} and $V_{PV2} < 1.1$ pu and both S_1 and S_2 < 1.5 pu_{pv}. Fig. 10 illustrates that using inverters with higher ratings, the proposed method can control the voltages within their limits even for a very weak load/grid.

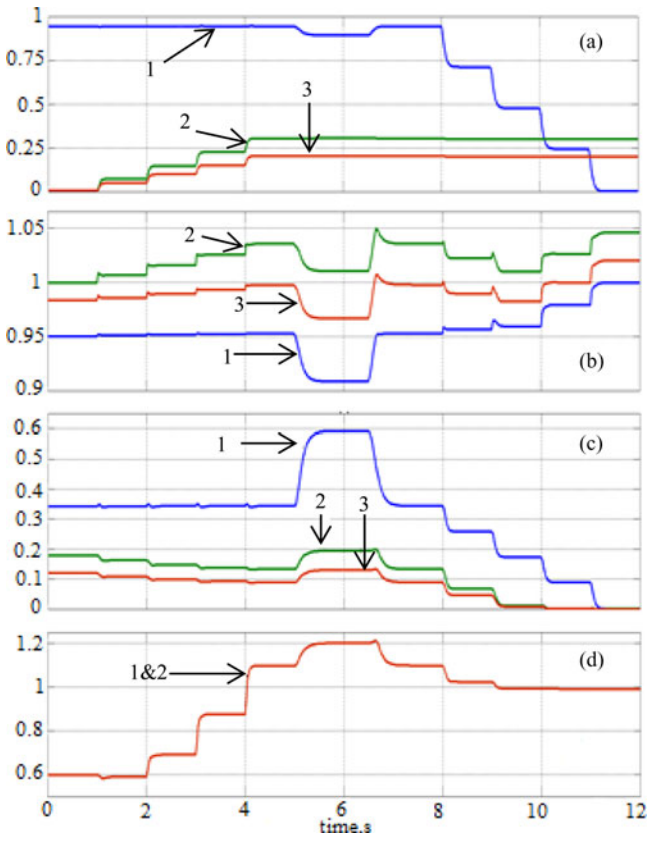

Fig. 9. Simulation results of two PV systems of $S_{nom} = 1.2$ pu_{pv} with the same solar irradiation (a) active power, pu 1-P_L, 2-P_{PV1}, 3-P_{PV2}, (b) voltage, pu 1-V_L, 2-V_{PV1}, 3-V_{PV2}, (c) reactive power, pu, 1-Q_L, 2-Q_{PV1}, 3-Q_{PV2}, and (d) magnitude of inverters apparent power, pu_{pv} 1-S_1, 2-S_2.

B. Different Step-Changed Solar Irradiations for PV Arrays

The sequence of simulation events, which is explained in Table IV, is similar to the previous one, except that P_{PV2} = 0, 0.5, 0.25, 1, 0.75 pu_{pv}.

Simulation results are illustrated in Fig. 11. It can be seen [see Fig. 11(c)] that when PF = 0.85 (t = 5–6.5 s), unlike the case with identical solar irradiation [see Fig. 9(c)], the reactive power is not shared in proportion to the rating of the converter (i.e., $Q_{PV1}/Q_{PV2} \neq$3/2). This is simply because P_{PV2} = 0.75 pu_{pv} while P_{PV1} = 1 pu_{pv}; hence, the second PV converter

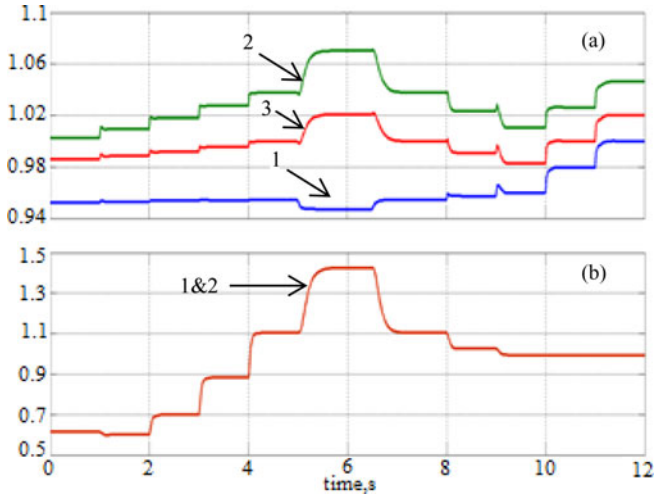

Fig. 10. Simulation results of two PV systems of $S_{\rm nom} = 1.5\ {\rm pu_{pv}}$ with the same solar irradiation (a) voltage, pu 1-V_L, 2-$V_{\rm PV1}$, 3-$V_{\rm PV2}$, and (b) magnitude of inverters apparent power, $\rm pu_{pv}$ 1-S_1, 2-S_2.

TABLE IV
SEQUENCE OF SIMULATION EVENTS FOR DIFFERENT IRRADIATION SCENARIO

Time, s	P_L, pu	P_{PV1}, $\rm pu_{pv}$	P_{PV2}, $\rm pu_{pv}$	Load PF
0-1	1	**0**	**0**	0.95
1-2	1	**0.25**	**0.5**	0.95
2-3	1	**0.5**	**0.25**	0.95
3-4	1	**0.75**	**1**	0.95
4-5	1	**1**	**0.75**	0.95
5-6.5	1	1	0.75	**0.85**
6.5-8	1	1	0.75	**0.95**
8-9	**0.75**	1	0.75	0.95
9-10	**0.5**	1	0.75	0.95
10-11	**0.25**	1	0.75	0.95
11-12	**0**	1	0.75	0.95

(the smaller one) has more capacity to supply Q than the first PV converter.

It is noted that for the rest of the simulation $Q_{\rm PV1}/Q_{\rm PV2} = 3/2$. It means that using this method, the inverters can compensate for one another if required (and, of course, if it is within its own limits).

As shown in Fig. 11(b), apart from when PF = 0.85, all voltages are controlled within their limits. It can be shown that using PV inverter with higher rating (similar to Fig. 10), $V_L >$ 0.94 pu even when PF = 0.85.

C. Different Real Solar Irradiations for PV Arrays

Fig. 12 shows the simulation results of model shown in Fig. 8 (with $S_{\rm nom} = 1.2\ {\rm pu_{pv}}$) while two real profiles of solar irradiation [see Fig. 12(a)] are applied to the PV arrays. The both solar irradiation profiles are measured at the College of Engineering, Swansea University, Swansea, U.K. (at 51.6100 northern latitude and 3.9797 western longitude). The measurements have been stored for almost one year and two days with largest variations in solar irradiation have been chosen for this simulation. The first profile is stored on 2/6/2011 and the second on 20/5/2011. The simulation starts with $P_L = 1$ pu [see Fig. 12(b)] and from $t = 300$ s, P_L reduces to zero in four steps. Fig. 12(c)

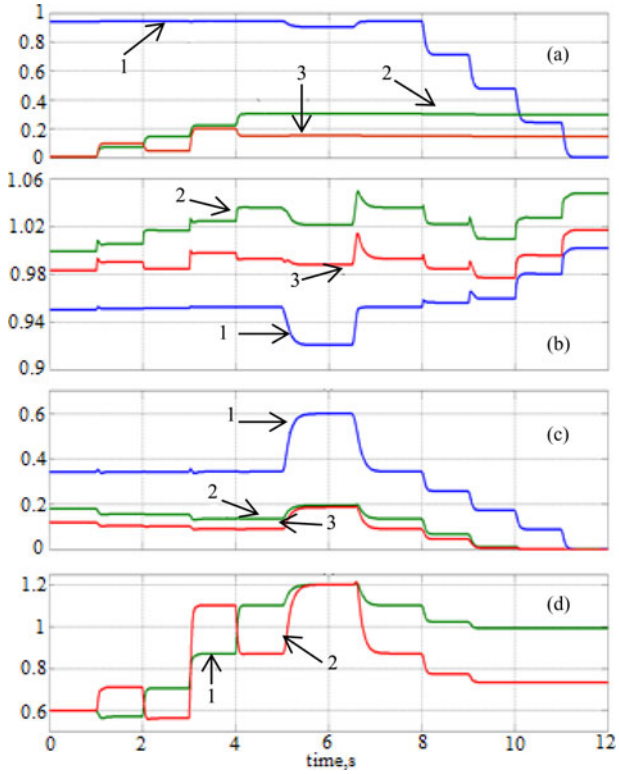

Fig. 11. Simulation results of two PV systems of $S_{\rm nom} = 1.2\ {\rm pu_{pv}}$ with different solar irradiation (a) active power, pu 1-P_L, 2-$P_{\rm PV1}$, 3-$P_{\rm PV2}$. (b) voltage, pu 1-V_L, 2-$V_{\rm PV1}$, 3-$V_{\rm PV2}$, (c) reactive power, pu, 1-Q_L, 2-$Q_{\rm PV1}$, 3-$Q_{\rm PV2}$, and (d) magnitude of inverters apparent power, $\rm pu_{pv}$ 1-S_1, 2-S_2.

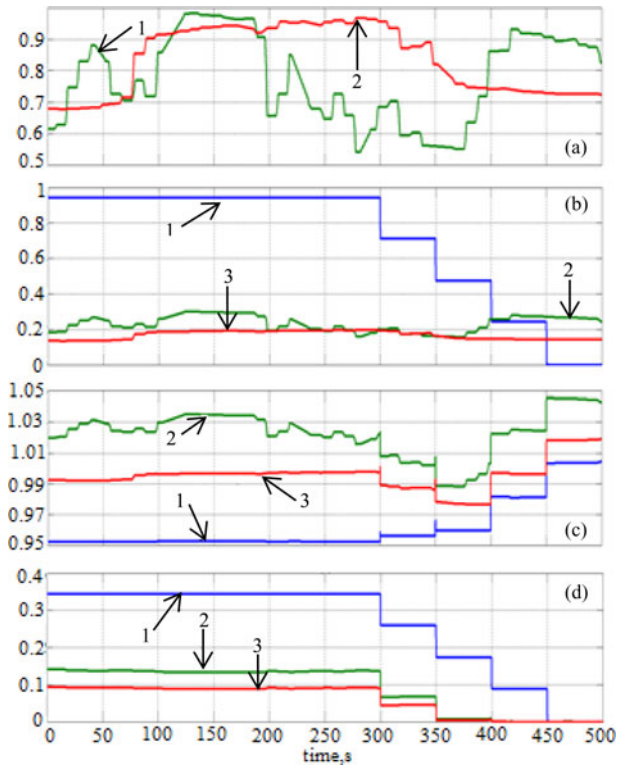

Fig. 12. Simulation results of two PV systems of $S_{\rm nom} = 1.2\ {\rm pu_{pv}}$ with real solar irradiation (a) solar irradiation, kW/m^2,1-PV1, 2-PV2, (b) active power, pu 1-P_L, 2-$P_{\rm PV1}$, 3-$P_{\rm PV2}$. (c) Voltage, pu 1-V_L, 2-$V_{\rm PV1}$, 3-$V_{\rm PV2}$, and (d) reactive power, pu 1-Q_L, 2-$Q_{\rm PV1}$, 3-$Q_{\rm PV2}$.

illustrates that V_L, V_{PV1}, and V_{PV2} are controlled within their limits. Fig. 12(d) shows that $Q_{\mathrm{PV1}}/Q_{\mathrm{PV2}} = 3/2$ even with real solar irradiation. It is noted that without the voltage support V_L would drop down to 0.87 pu.

VIII. Conclusion

The paper presents a small-signal model for a PV inverter exchanging reactive power with the grid and investigates its stability using the model. A simple and yet effective voltage control using the PV inverter(s) has been proposed and validated using PSCAD/EMTDC simulations. It has been shown that the method utilizes all the available capacity of the PV inverter (when it is needed) without violating the rating of the converter and the maximum voltage the inverter's switching device can withstand. The method has been validated for multiple PV arrays and it was shown that (in normal operation) the reactive power is shared proportional to PV ratings. However, if the rating of one of the inverters is hit, the other inverter can generate more reactive power (if the capacity is available) to support the voltage. The method has been also validated with real (measured) solar irradiation.

References

[1] M. Fazeli, G. Asher, C. Klumpner, and L. Yao, "Novel integration of wind generator-energy storage systems within microgrids," *IEEE Trans. Smart Grid*, vol. 3, no. 2, pp. 728–737, Jun. 2012.

[2] Z. Jiang and X. Yu, "Power electronics interfaces for hybrid DC and AC-linked microgrids," presented at the 6th Int. Power Electron. Motion Control Conf., Wuhan, China, 2009.

[3] M. I. Marie, E. F. El-Saadany, and M. M. A. Salama, "An intelligent control for the DG interface to mitigate voltage flicker," presented at the IEEE 18th Annu. Appl. Power Electron. Conf., 2003.

[4] C. Wang and M. H. Nehrir, "Analytical approaches for optimal placement of distributed generation sources in power systems," *IEEE Trans. Power Syst.*, vol. 19, no. 4, pp. 2068–2076, Nov. 2004.

[5] M. Fazeli, G. Asher, C. Klumpner, and L. Yao, "Novel integration of DFIG-based wind generators within microgrid," *IEEE Trans. Energy Convers.*, vol. 26, no. 3, pp. 840–850, Sep. 2011.

[6] K. Turitsyn, P. Sulc, S. Backhaus, and M. Chertkov, "Options for control of reactive power by distributed photovoltaic generation," *Proc. IEEE*, vol. 99, no. 6, pp. 1063–1073, Jun. 2011.

[7] R. Yan and T. K. Saha, "Investigation of voltage stability for residential customers due to high photovoltaic penetration," *IEEE Trans. Power Syst.*, vol. 27, no. 2, pp. 651–661, May 2012.

[8] T. Senjyu, Y. miyazato, A. Yona, N. Urasaki, and T. Funabashi, "Optimal distribution voltage control and coordination with distributed generation," *IEEE Trans. Power Del.*, vol. 23, no. 2, pp. 1236–1242, Apr. 2008.

[9] R. O'Gorman and M. Redfern, "The impact of distributed generation on voltage control in distribution systems," presented at the 18th Int. Conf. Elect. Distrib., Turin, Italy, Jun. 2005.

[10] M. A. Eltawil and Z. Zhao, "Grid-connected photovoltaic power systems: Technical and potential problems—A review," *Renewable Sustainable Energy Rev.*, vol. 14, pp. 112–129, 2010.

[11] S. Chalmers, M. Hitt, J. Underhill, and P. Anderson, "The effect of photovoltaic power generation on utility operation," *IEEE Trans. Power App.*, vol. PA-104, no. 3, pp. 2020–2024, Mar. 1985.

[12] V. Quezada, J. Abbad, and T. S. Roman, "Assessment of energy distribution losses for increasing penetration of distributed generation," *IEEE Trans. Power Syst.*, vol. 21, no. 2, pp. 533–540, May 2006.

[13] M. Thomson and D. Infield, "Impact of widspread photovoltaic generation on distribution systems," *IET Renewable Power Gen.*, vol. 1, no. 1, pp. 33–40, Mar. 2007.

[14] K. Turitsyn, P. Sulc, and S. Backhaus, "Use of reactive power flow for voltage stability control in a radial circuit with photovoltaic generation," presented at the IEEE Power Eng. Soc. Gen. Meet., Minneapolis, MN, USA, Jul. 2010.

[15] N. Mohan, T. M. Undeland, and W. P. Robbines, *Power Electronics*, 3rd ed. Hoboken, NJ, USA: Wiley, 2003, pp. 228–230.

[16] H. G. Yeh, D. F. Gayme, and S. H. Low, "Adaptive VAR control for distribution circuits with photovoltaic generators," *IEEE Trans. Power Syst.*, vol. 27, no. 3, pp. 1656–1663, Aug. 2012.

[17] P. Jahangiri and D. C. Aliprantis, "Distributed Volt/VAr control by PV inverters," *IEEE Trans. Power Syst.*, vol. 28, no. 3, pp. 3429–3439, Aug. 2013.

[18] M. Fazeli, P. Igic, and P. Holland, "Novel maximum power point tracking with classical cascaded voltage and current loops for photovoltaic systems," presented at the Renewable Power Gen., Edinburgh, U.K., Sep. 2011.

[19] E. Figueres, G. Garcera, J. Sandia, F. Gonzalez-Espin, and C. J. Rubio, "Sensitivity study of the dynamics of three-phase photovoltaic inverters with an LCL grid filter," *IEEE Trans. Ind. Electron.*, vol. 56, no. 3, pp. 706–717, Mar. 2009.

[20] N. Jenkins, J. B. Ekanayake, and G. Strbac, *Distributed Generation*, Institution of Engineering and Technology, U.K., 2010, pp. 84–88.

[21] A. Yazdani and P. P. Dash, "A control methodology and characterization of dynamics for photovoltaic (PV) system interfaced with a distribution network," *IEEE Trans. Power Del.*, vol. 24, no. 3, pp. 1538–1551, Jul. 2009.

[22] M. Liserre, F. Blaabjerg, and S. Hansen, "Design and control of an LCL-filter-based three-phase active rectifier," *IEEE Trans. Ind. Appl.*, vol. 41, no. 5, pp. 1281–1291, Oct. 2005.

Meghdad Fazeli (M'13) received the B.Sc. degree in electrical engineering from the Chamran University of Ahwaz, Iran, in 2004, the M.Sc. degree in electrical engineering and the Ph.D. degree in wind generator-energy storage control schemes for autonomous grids both from Nottingham University, U.K., in 2006 and 2010, respectively.

Since January 2011, he has been with the Swansea University, U.K. He has appointed as a Lecturer in Electrical Power Engineering since September 2013. His current research is mainly concentrated on grid integration of photovoltaic systems. His main research interests include the integration of renewable energy resources with grids, smartgrids, and distributed generation.

Janaka Ekanayake (S'93–M'95–SM'02) was born in Matale, Sri Lanka, on October 9, 1964. He received the B.Sc. degree in electrical engineering from the University of Peradeniya, Sri Lanka, and the Ph.D. degree from the University of Manchester Institute of Science and Technology, U.K.

Just after the Ph.D. degree, he joined the University of Peradeniya as a Lecturer and he was promoted to a Professor in electrical engineering in 2003. In 2008, he joined the Cardiff School of Engineering, U.K. His main research interests include power electronic applications for power systems, renewable energy generation and its integration. He has published more than 25 papers in refereed journals and has also coauthored three books.

Dr. Ekanayake is a Fellow of the IET.

Paul M. Holland (M'12–M'14) received the B.Sc. degree (with Hons.) in engineering physics from Sheffield Hallam University, U.K., in 1993, and the Ph.D. degree in power integrated circuit technology development at Swansea University, U.K., in 2007.

He spent the first ten years of his career working in the U.K. semiconductor industry for GEC Plessey and ESM Ltd., as a Senior Process and a Device Engineer. After working as a Researcher at Swansea University from 2002, he was appointed as a Lecturer in 2008 in the College of Engineering and now a Senior Lecturer. His research interests include renewable energy technologies, power IC technologies and CMOS Lab-On-A-Chip develop development which is funded by the Engineering and Physical Sciences Research Council. He recently helped develop the National Strategy for Power Electronics in the U.K. working with the leading academics in this area, industry and the U.K. government.

Petar Igic (M'13) received the Dipl.-Eng. and Mag.Sc. degrees from the University of Nis, Serbia, and the Ph.D. degree from Swansea University, U.K.

He is the Head/Director of the Electronic Systems Design Centre at Swansea University, U.K. and is a Reader at the College of Engineering. He has 20 year experience of research in power electronics and semiconductor devices and technologies. He worked on industrial projects or been a consultant to several major Japanese, European, and American multinationals, such as TOYOTA, HITACHI, SILICONIX, ALSTOM, X-Fab, Diodes-ZETEX, etc. He has published and presented more than 100 scientific papers in journals and international conferences.